

Direct contact packed bed thermal gradient attenuators: Theoretical analysis and experimental observations

Kevin M. Lawton, Steven R. Patterson,^{a)} and Russell G. Keanini
*Center for Precision Metrology, Department of Mechanical Engineering and Engineering Science,
University of North Carolina at Charlotte, Charlotte, North Carolina 28223*

(Received 2 January 2003; accepted 26 January 2003)

This article theoretically and experimentally characterizes direct contact, packed bed thermal gradient attenuators in which a fluid control stream, subject to broadband thermal disturbances, flows through a thermally attenuating packed bed medium. The theoretical model decomposes the device into three subsystems: an upper mixing volume, the packed bed, and a lower mixing volume. Analysis of the packed bed subsystem leads to a coupled system of equations that describe local heat transfer within the control stream and within individual spherical elements comprising the packed bed; the system of equations obtained has the same general form as that derived in an earlier investigation of tube-in-shell, noncontact thermal gradient attenuators [J. Heat Transfer **123**, 796 (2001)]. Associated subsystem transfer functions are derived, and in analogy with observations reported in the earlier investigation, are shown to provide simple, unambiguous criteria for designing and optimizing packed bed attenuators. It is found that, for 52 different sets of experimental conditions, theoretical performance of the device matches experimental performance to within 2.5 dB root mean square, and that the device provides several orders of magnitude attenuation for flow rates on the order of 1 l/min and disturbance frequencies higher than approximately 10 mHz. The results of the present study and the earlier investigation together provide a useful basis for analyzing and designing large and small, contacting and noncontacting, thermal gradient attenuators. © 2003 American Institute of Physics. [DOI: 10.1063/1.1564279]

I. INTRODUCTION

Thermal gradient attenuators comprise a key element in precision temperature control systems,¹⁻³ and are designed to attenuate thermal spectral components in fluid control streams that exceed a nominally defined minimum frequency, f_{\min} . Temperature oscillations slower than f_{\min} pass through for compensation by low-bandwidth heater controllers.² The devices use available chilled water supplies to provide high-stability chilled water sources for subsequent system thermal control.

Recent work¹ has focused on theoretically and experimentally characterizing large tube-in-shell attenuators in which the chilled water control stream passed through a bank of plastic tubes immersed in a large, stagnant volume of water, where the latter served as the attenuating medium. A closed-form, lumped-differential heat transfer model of the system was shown to accurately predict system performance over more than two decades of disturbance frequency and over a wide range of control stream flow rates. More importantly, the model developed in Ref. 1 led to simple design criteria that could be used to design tube-in-shell attenuators as well as tune and optimize existing devices.

Techniques for obtaining precision temperature control near room temperature fall into one of three broad classes: methods that employ resistive heaters to maintain a small enclosure near ambient,³⁻¹⁰ methods that use a stagnant fluid

to heat or cool an enclosure,¹¹⁻¹⁴ and techniques that rely on a recirculating fluid stream to maintain control of the temperature.^{1,15-18} See Ref. 1 for a brief overview. Surprisingly, little theoretical work has been carried out to support the design and development of precision temperature control devices.^{1,19,20} Although formulation of accurate, predictive thermal and system models can be difficult,^{5,19} and has led to development of various anecdotal criteria for designing thermal control devices, the potential advantages of formulating such models are significant: (i) existing devices can be tuned to meet specific performance requirements, (ii) potential designs can be tested theoretically prior to construction, (iii) methods for improving device performance can be unambiguously determined and implemented, and (iv) system behavior can be interpreted and modified or controlled as needed.

The objective of the present study is to theoretically and experimentally characterize direct contact, packed bed attenuators. In the device to be studied, a control stream passes through a spatially compact, attenuating packed bed of stainless steel spheres. As in the earlier investigation,¹ which focused on large, noncontact tube-in-shell attenuators, theoretical heat transfer and system models lead to unambiguous and readily implemented criteria for designing packed bed attenuators. Together, the results of the present and previous¹ investigations should provide a useful basis for designing and analyzing large and small, contacting and noncontacting thermal gradient attenuators.

^{a)}Author to whom correspondence should be addressed; electronic mail: spatters@uncc.edu

II. GENERIC DESIGN REQUIREMENTS AND DESCRIPTION OF THE DEVICE

Two generic design requirements were defined at the outset. First, since the tube-in-shell device developed in Ref. 1 was relatively large (200 l total volume) and of complex construction, it was desired to enhance its portability by reducing the device volume, and to improve its utility by simplifying construction. Second, to allow ready modification of the performance characteristics of the device, modular designs were examined in which the heat capacity of the attenuating medium, C_a , and the effective total thermal resistance of the device, R , could be easily altered. In defining this second requirement, guidance was provided by the theoretical design criteria derived in the first study¹ which showed that for a fixed flow rate through a *tube-in-shell* attenuator (i) asymptotic attenuation, i.e., the maximum attainable attenuation, was inversely proportional to the overall thermal resistance, R , between the control stream and attenuating medium, and (ii) for an R value that meets a desired asymptotic attenuation requirement, the minimum input disturbance frequency, f_{\min} , asymptotically attenuated shifted toward lower magnitudes with an increase in attenuating medium heat capacity, C_a .

Thus, in order to achieve maximal asymptotic attenuation within a spatially compact design or, more specifically, in order to reduce thermal resistance between the control stream and attenuating medium, a direct contact approach was chosen in which the control stream flowed through a fixed, packed bed of attenuating media. This approach is in marked contrast to that used in Ref. 1 where a large attenuator time constant was required in order to attenuate sub-MHz disturbance frequencies. As detailed in that paper, and as discussed below, the attenuator time constant, τ_a , given by $\tau_a = RC_a$, can be tuned by varying R and/or C_a . Thus, as a means of obtaining large τ_a in Ref. 1, R was maximized by passing the control stream through a bank of low conductivity plastic tubes immersed in a stagnant attenuating medium (water), while C_a was maximized by employing a large volume of the high specific heat attenuating medium.

Here, having chosen a direct contact approach for minimizing R , methods were explored for maximizing the range of disturbance frequencies subject to asymptotic attenuation, i.e., methods were sought for maximizing τ_a . In order to satisfy generic design requirements of compactness and tunability, a relatively low-cost, easily handled solid attenuating material having high density and high specific heat was sought; stainless steel spheres met these requirements well. With regard to tunability, it will be shown below that the overall thermal resistance R is inversely proportional to the number of spheres, N , within the column, and in addition, depends on the radius, r_s , and thermal conductivity, k_a , of the spheres. Similarly, the attenuating medium total heat capacity, C_a , will be shown to depend on N , the overall radius of the bed, r_0 , and the specific heat and density of the attenuating medium, c_a and ρ_a , respectively. Thus, given the number of parameters that can be adjusted to effect changes in R and C_a , a packed bed design meets tunability requirements well.

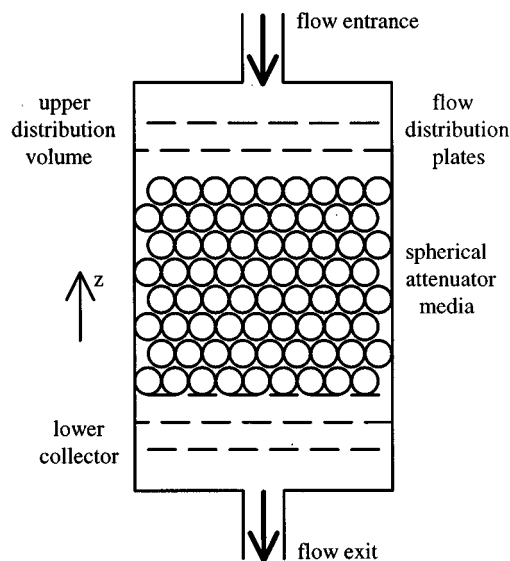


FIG. 1. Packed bed thermal gradient attenuator configuration.

The final design is depicted schematically in Fig. 1. As shown, the device consists of a cylindrical packed bed of stainless steel spheres, an upper distribution volume, and a lower collector. The upper distribution volume, designed to mix and spread the incoming control stream uniformly over the top of the packed bed, contains, in succession, a coarsely perforated plastic plate, a finely perforated plastic plate, and a fine mesh screen. Holes in the course plate are 3 mm in diameter (25 mm center-to-center spacing), while those in the fine plate are 1.5 mm in diameter (12.5 mm center-to-center spacing); the wire mesh is plastic window screen. The two plates and screen are each spaced 25 mm apart. A similar arrangement is used in the lower collector volume. A cylindrical plastic (PVC) canister, either 100 or 150 mm in diameter, comprises the housing for the upper distribution volume, the packed bed media, and the lower collector volume.

III. PACKED BED ATTENUATOR THERMAL MODEL

For modeling purposes, the device will be decomposed into three subsystems: the packed bed, the upper distribution volume, and the lower collector. Here in Sec. III, the coupled system of equations that describe heat transfer within the stream and the individual spheres comprising the packed bed is derived. Although the modes of heat transfer and flow extant in the packed bed device differ radically from those in the tube-in-shell device studied in Ref. 1, it will nevertheless develop that both systems are governed by systems of equations having the same generic form. Given this result, derivation of the associated packed bed transfer function (given in detail in Sec. IV) follows immediately from the earlier work.

A. Qualitative flow and heat transfer features

In the derivation to follow (Sec. III B), heat transfer between the fluid and attenuating spheres occupying a horizontal cross section of thickness, Δz , will be considered. In order to provide a conceptual framework for the analysis,

here in Sec. III A we will first describe the important time scales that characterize heat transfer within the slice. Subsequently, a simple physical picture of in-bed heat transfer will be described.

Three distinct time scales characterize in-bed heat transfer: (i) The convective time scale, $\tau_c = r_s/w_s$, characterizes two processes: the time required for infinitesimal fluid elements to mix and thus smooth local fluid temperature gradients, and the time required for fluid to pass over any given sphere. Here, w_s , the characteristic fluid velocity scale within the bed, is taken to be the superficial velocity, $w_{sup} = \dot{m}/(\rho_f \pi r_0^2)$, i.e., the fluid velocity extant in the absence of packing material, where \dot{m} is the control stream mass flow rate and ρ_f is the fluid density. (ii) The thermal diffusion time scale, $\tau_D = r_s^2/\alpha_a$, characterizes the time required for variations in temperature to smooth within individual spheres and it is an order of magnitude longer than τ_c . [In particular, for the range of experimental conditions considered here, w_s and r_s are on the order $1 \times 10^{-2} \text{ m s}^{-1}$ and $3 \times 10^{-3} \text{ m}$, respectively, while $\alpha_a \approx 4 \times 10^{-6} \text{ m}^2 \text{ s}^{-1}$; thus, $\tau_c \approx 0.1 \text{ s}$ and $\tau_D \approx 2 \text{ s}$.] (iii) The disturbance time scale, $\tau_i = f_i^{-1}$, is, at least in the present investigation, the longest and is determined by the highest (significant) frequency in the spectrum of the untreated stream. As shown in Ref. 1, the spectrum of the unattenuated flow (obtained from an in-house chilled water source) is dominated by spectral features at frequencies less than 0.1 Hz;¹ f_i is thus taken as 0.1 Hz.

Given the above separation in time scales, and given that the control stream is well mixed within the upper distribution volume prior to being uniformly distributed over the top of the bed, the following physical picture emerges. (1) On time scales longer than τ_c , but shorter than, or on the order of τ_D , fluid temperatures within any given horizontal slice are spatially uniform in both the radial direction and across the slice thickness, Δz . (2) Due to both the relatively slow variations in temperature at the device inlet (occurring on time scales on the order of f_i^{-1}), and the short convective time scale, τ_c , all spheres within the slice are bathed in the same spatially uniform, though slowly time-varying fluid temperature field. The derivation to follow is based on these simple physical considerations.

B. Packed bed heat transfer model

Consider steady downward flow of an incompressible control fluid through the packed bed shown in Fig. 1. An energy balance on the fluid within a thin horizontal cross section of thickness Δz leads to

$$\begin{aligned} \rho_f c_f \frac{\partial}{\partial t} \int_{\Delta V} T_f dV &= \rho_f c_f \int_A w T_f dA|_z \\ &- \rho_f c_f \int_A w T_f dA|_{z+\Delta z} \\ &+ \sum_{j=1}^n \left[\int_{A_s} h_j (T_w^j - T_f) dA \right], \end{aligned} \tag{1}$$

where terms from left to right represent, respectively, the rate of change of fluid enthalpy within the slice, the total flux of

enthalpy into the slice at z , the total flux of enthalpy out at $z + \Delta z$, and the total rate of convective heat transfer between the fluid and spheres within the slice. Here, ρ_f and c_f are the fluid density and specific heat, respectively, $\Delta V = \pi r_0^2 \Delta z$ is the slice volume, $A = \pi r_0^2$ is the cross-sectional area of the bed, r_0 is the radius of the packed bed, $A_s = 4 \pi r_s^2$ is the surface area of any given sphere, n is the number of spheres within the slice, h_j and T_w^j are the local convective heat transfer coefficient and surface temperature of the j th sphere within the slice, respectively, and T_f is the local fluid temperature.

Based on the physical considerations in Sec. III A, radial variations in temperature within the slice are neglected. By Taylor expansion of the outflow flux term in Eq. (1) about z and noting that $T_f = T_f(z, t) = \bar{T}_f(z, t)$, where $\bar{T}_f = A^{-1} \int_A T_f dA$ is the area averaged (or radially lumped) fluid temperature, the net flux of enthalpy through the slice is then given by

$$\rho_f c_f \Delta z \frac{\partial}{\partial z} \int_A w T dA = \rho_f c_f \Delta z \frac{\partial}{\partial z} \bar{w} \bar{T}_f A, \tag{2}$$

where \bar{w} is the area averaged vertical velocity component. Note that A , the area available for flow, is related to the packed bed cross-sectional area via $A = \epsilon A_0$, where ϵ is the void fraction.

Considering next the net heat transfer rate between the fluid and the attenuating spheres within the slice, it is noted that variations in inlet temperature are small, on the order of 1 K or less. Thus, h_j is assumed constant both within the slice and throughout the entire packed bed. Likewise, since spatial in-fluid temperature variations within the slice are small, it is assumed that the surface temperature, T_w^j , is spatially uniform over each sphere in the slice and, additionally, that the instantaneous magnitude of T_w^j is the same for every sphere in the slice. Thus, $T_w^j = \bar{T}_w(z, t)$, where $\bar{T}_w(z, t) = (n A_s)^{-1} \int_{A_s} T_w^j dA$. Using $T_f = \bar{T}_f = \bar{T}_f(z, t)$, the total heat transfer rate between the spheres and fluid within the slice assumes the form of

$$\sum_{j=1}^n \left[\int_{A_s} h_j (T_w^j - T_f) dA \right] = n h A_s [\bar{T}_w(z, t) - \bar{T}_f(z, t)], \tag{3}$$

where h is the (constant) heat transfer coefficient.

Noting that the number of spheres within the slice is given by $n = N \Delta z / L$, where L is the bed length, and that

$$\rho_f c_f \frac{\partial}{\partial t} \int_{\Delta V} T_f = \rho_f c_f \Delta z \epsilon A_0 \frac{\partial}{\partial t} (\bar{T}_f),$$

it is found, using Eqs. (2) and (3) in Eq. (1), that the radially lumped energy balance across the slice assumes the form:

$$\begin{aligned} \rho_f c_f \epsilon A_0 \Delta z \left(\frac{\partial}{\partial t} (\bar{T}_f) + \bar{w} \frac{\partial}{\partial z} \bar{T}_f \right) \\ = -N 4 \pi r_s^2 h [\bar{T}_f(z, t) - \bar{T}_w(z, t)] \frac{\Delta z}{L}. \end{aligned} \tag{4}$$

Notice that \bar{w} is assumed to be independent of z ; this follows from mass conservation of the control stream and from the assumption that the fluid completely fills all voids within the bed.

In deriving Eq. (4), it is implicitly assumed that the thickness of the slice, Δz , is on the order of the sphere radius, r_s , i.e., axial temperature variations within the bed are assumed to occur on length scales larger than r_s . Again, since the convective time scale, τ_c , for fluid flow over any given sphere is short relative to the incoming disturbance (τ_i) and in-sphere thermal diffusion (τ_D) time scales, then on the latter time scale, every sphere within a slice having thickness $\Delta z = O(r_s)$ is exposed to a spatially uniform, although slowly time-varying, fluid temperature. Thus, on the thermal diffusion time scale of the spheres, axial fluid temperature gradients over distances on the order of r_s are negligible.

Having determined the radially lumped equation that governs heat transfer within the fluid in a given horizontal slice, heat transfer within individual spheres within the slice is now considered. Since the surface temperature of each sphere within the slice is spatially uniform, although time varying, the temperature within the sphere depends only on time and radial position r within the sphere. The equation that governs conduction within the sphere is thus given by

$$\frac{\partial T_a}{\partial t} = \alpha_a \frac{1}{r^2} \frac{\partial^2 T_a}{\partial r^2},$$

where α_a is the thermal diffusivity of the sphere, and subscript a refers to the properties of the attenuating spheres. Multiplying both sides by $N\Delta z/L4\pi r^2$ and integrating over the sphere volume yields

$$\frac{4}{3} n \pi r_s^3 \rho_a c_a \frac{\partial \bar{T}_a}{\partial t} = N k_a 4 \pi r_s^2 \left. \frac{\partial \bar{T}_a}{\partial r} \right|_{r_s} \frac{\Delta z}{L}, \quad (5)$$

where \bar{T}_a is the volume averaged temperature within each sphere. Now note that the right-hand side of Eq. (5) is identically equal to the right-hand side of Eq. (4), i.e., the total instantaneous rate of convective heat transfer to or from the spheres within the slice [given by the right-hand side of Eq. (4)] must equal the total rate of conductive heat transfer into or out of the spheres within the slice [as given by the right-hand side of Eq. (5)].

Defining the right-hand sides of Eqs. (4) and (5) as $Q(z, t)$, and using the network analogy,²¹ Q can be expressed as

$$Q(z, t) = \frac{T_w - T_c}{R_{\text{cond}}} \left(\frac{\Delta z}{L} \right) = \frac{\bar{T}_f - T_w}{R_{\text{conv}}} \left(\frac{\Delta z}{L} \right), \quad (6)$$

where

$$R_{\text{cond}} = \frac{1}{4\pi k_a N} (r_c^{-1} - r_s^{-1}) \quad (7)$$

is the total conductive thermal resistance associated with the spheres in the packed bed and

$$R_{\text{conv}} = \frac{1}{4\pi r_s^2 N h} \quad (8)$$

is the total convective thermal resistance between the fluid and spheres within the bed. The expression for R_{cond} is obtained using the spherical shell model²² in which the steady conduction equation within any given sphere is integrated from a radius r_c , enclosing half the volume of the sphere, to r_s ; here, the temperature at r_c is denoted as T_c . Since incoming temperature variations (at the device inlet) are relatively small (with magnitudes on the order of 1% of the mean), variations in temperature within each sphere are likewise small; thus, the effective conductive resistance can be accurately derived via this approach.¹

In order to determine the convective resistance, R_{conv} , h is estimated using the following correlation, valid for convective heat transfer in packed beds:²¹

$$h = 0.455 \epsilon^{-1} \text{Re}_D^{-0.4} Pr^{-2/3} c_f \rho_f w_{\text{sup}}, \quad (9)$$

where Pr is the fluid Prandtl number, $\text{Re}_D = \rho_f w_{\text{sup}} D_p / \mu_f$ is the Reynolds number, D_p is the effective diameter, and μ_f is the fluid viscosity. The correlation was developed using cylindrically shaped bedding elements; introduction of the effective diameter, defined as $D_p = A_s^{1/2} \pi^{-1/2}$, allows application of the correlation to packed beds containing noncylindrical elements.²¹ The relationship is valid for $0.371 \leq \epsilon \leq 0.451$ and $10 \leq \text{Re}_D \leq 200$ where, in the present study, ϵ and Re_D are approximately 0.38 and 50, respectively.

Next, and as a convenience in interpreting system dynamics, fluid and attenuator time constants are defined as $\tau_f = RC_f$ and $\tau_a = RC_a$, respectively, where $R = R_{\text{conv}} + R_{\text{cond}}$ is the total thermal resistance between the fluid and spheres, $C_f = \epsilon A_0 L \rho_f c_f$ is the total thermal capacity of the fluid within the bed, and $C_a = N \frac{4}{3} \pi r_s^3 \rho_a c_a$ is the total thermal capacity of the packed bed attenuating medium. Using Eq. (6) and the above definitions, Eqs. (4) and (5) can then be expressed as

$$\frac{\partial \bar{T}_f}{\partial t} + \bar{w} \frac{\partial \bar{T}_f}{\partial z} = \frac{1}{\tau_f} (\bar{T}_a - \bar{T}_f) \quad (10)$$

and

$$\frac{\partial \bar{T}_a}{\partial t} = \frac{1}{\tau_a} (\bar{T}_f - \bar{T}_a), \quad (11)$$

respectively, where the common factor Δz has been divided out of Eq. (4) and where T_c in Eq. (6) has been approximated as the volume averaged temperature within a given sphere, $T_c(z, t) \approx \bar{T}_a(z, t)$. [Again, due to the smallness of the variations in incoming temperature, this is a reasonable approximation.]

IV. SUBSYSTEM TRANSFER FUNCTIONS

A. Packed bed transfer function

The lumped system of equations that describes coupled heat transfer between the control stream and the attenuating packed bed medium, Eqs. (10) and (11), is identical in form to that derived for noncontact tube-in-shell thermal gradient attenuators.¹ Thus, following the development in Ref. 1, the following dimensionless space and time variables,

$$\eta = z / (\bar{w} \tau_a) \quad \text{and} \quad \tau = t / \tau_a,$$

dimensionless heat capacity ratio,

$$\zeta = \tau_a / \tau_f = C_a / C_f,$$

and dimensionless radially averaged temperatures,

$$\theta_f = \bar{T}_f / T_0 \quad \text{and} \quad \theta_a = \bar{T}_a / T_0,$$

may be substituted into Eqs. (10) and (11) to obtain

$$\frac{\partial \theta_f}{\partial \tau} + \frac{\partial \theta_f}{\partial \eta} = \zeta(\theta_a - \theta_f) \quad (12)$$

and

$$\frac{\partial \theta_a}{\partial \tau} = (\theta_f - \theta_a), \quad (13)$$

where T_0 is a convenient characteristic temperature, e.g., the mean temperature at the inlet to the device. Taking the Laplace transforms of Eqs. (12) and (13), with initial conditions equal to zero, then yields

$$s \hat{\theta}_f + \frac{\partial \hat{\theta}_f}{\partial \eta} = \zeta(\hat{\theta}_a - \hat{\theta}_f) \quad (14)$$

and

$$s \hat{\theta}_a = (\hat{\theta}_f - \hat{\theta}_a), \quad (15)$$

where $s = 2i\pi f\tau_a$, and f is the frequency in Hz. Eliminating $\hat{\theta}_a$ from this system then leads to

$$\frac{\partial \hat{\theta}_f}{\partial \eta} + \frac{s}{s+1}(s+\zeta+1)\hat{\theta}_f = 0. \quad (16)$$

Finally, solving Eq. (16) for $\hat{\theta}_f$ yields the transfer function for the packed bed portion of the attenuator:

$$\begin{aligned} Tr_{a}(s) &= \frac{\hat{\theta}_f(\eta = \eta_L, s)}{\hat{\theta}_f(\eta = 0, s)} \\ &= \exp\left[\frac{-s}{s+1}(s+\zeta+1)\eta_L\right] \\ &= \exp\left[\frac{-s\zeta\eta_L}{s+1}\right] \exp[-s\eta_L], \end{aligned} \quad (17)$$

where the effect of transport delay, $\exp(-s\eta_L)$, is separated out. Since only the real part of the exponent affects the magnitude of the transfer function, the packed bed transfer function magnitude, $Trm_a(s)$, can be expressed in the form of

$$Trm_a(s) = \exp\left[-\zeta\eta_L \operatorname{Re}\left(\frac{s}{s+1}\right)\right]. \quad (18)$$

B. Theoretical design criteria: Packed bed subsystem

Equation (18) is an important result since it encapsulates theoretical criteria for designing the packed bed portion of the attenuator. In particular, two design parameters, the asymptotic attenuation and the range of input disturbance frequencies subject to asymptotic attenuation, comprise the primary design features to be considered in designing the packed bed subsystem. Considering first asymptotic attenuation, by letting $f \rightarrow \infty$ (or, equivalently, by letting $s \rightarrow \infty$) in Eq. (18), it is found that this parameter is proportional to

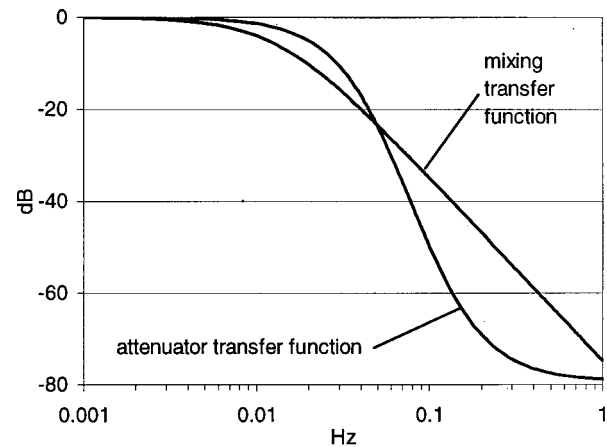


FIG. 2. Theoretical transfer function for packed bed subsystem (labeled attenuator transfer function) compared with combined theoretical transfer functions of upper distribution volume and lower collector (labeled as mixing transfer function), assuming a 100 mm diam tube, 3.8 l/min flow rate, and 10 000 6.4 mm spheres.

$\exp(-\zeta\eta_L) = \exp[-(C_a/C_f)\eta_L]$. Thus, for a given dimensionless bed length, η_L , the heat capacity ratio, ζ , determines the magnitude of asymptotic attenuation. Alternatively, by expressing $\eta_L\zeta$ in terms of dimensional variables,

$$\eta_L\zeta = \frac{1}{\dot{m}c_fR}, \quad (19)$$

it is seen that for a given mass flow rate, \dot{m} , and specific heat, c_f , the asymptotic attenuation is determined by the total thermal resistance, R , between the control stream and the attenuating packed bed medium.

Considering the range of frequencies asymptotically attenuated within the packed bed, by expressing (18) in terms of dimensional variables,

$$Trm_a(f) = \exp\left[-\frac{1}{\dot{m}c_fR} \operatorname{Re}\left(\frac{2i\pi f\tau_a}{2i\pi f\tau_a + 1}\right)\right], \quad (20)$$

it is seen that this range increases as τ_a increases. More specifically, by computing the real part of the second term in the exponent above, it is readily shown that for all frequencies satisfying $f \geq \tau_a^{-1}$, the exponent is within 2.5% of its asymptotic limit. Thus, the minimum disturbance frequency, f_{\min} , subject to asymptotic attenuation within the packed bed portion of the device can be conveniently approximated as

$$f_{\min} \approx \tau_a^{-1}.$$

It is important to note that in the present device, due to the relatively large volumes of the upper distribution volume and lower collector, attenuation within these subsystems is comparable to, and over low frequencies ($f \lesssim 0.015$ Hz), larger than, that obtained over the packed bed. This feature is illustrated in Fig. 2 which plots the logarithm of the transfer functions (in dB) for the packed bed and the combined upper and lower volumes (under typical experimental conditions). [In the following, the logarithm of any given transfer function will be generically referred to as “attenuation.”] While total system attenuation is the additive sum of the attenuation obtained over each subsystem, in cases where the upper and

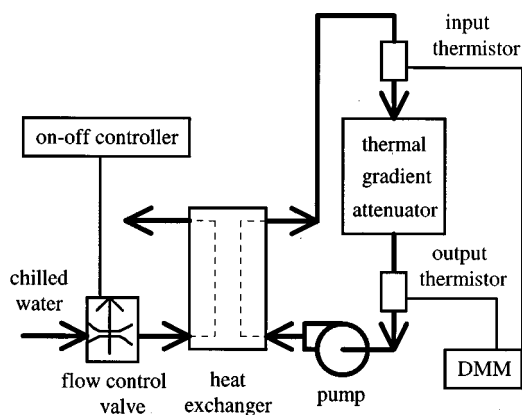


FIG. 3. Thermal gradient attenuator test setup with an on-off chilled water flow controller generating sinusoidal temperature oscillations in the test stream, measured by thermistors connected to a digital multimeter.

lower volumes are small compared to the packed bed volume, then similar to the observations reported in Ref. 1, system behavior and design can be adequately described using the packed bed transfer function alone, Eq. (20).

C. Upper distribution volume and lower collector transfer functions

Since additional attenuation occurs within the upper distribution and lower collector volumes, corresponding transfer functions must be determined in order to model total system performance. The control stream enters the upper volume as a single jet (7 mm in diameter) and then flows over and through the perforated distribution plates. Likewise, flow in the lower volume passes over additional distribution plates before exiting. Thus, both volumes are modeled as perfectly mixed,¹ leading to the following subsystem transfer function for each:¹

$$Tr_m(f) = \frac{1}{1 + \tau_m 2i\pi f}, \quad (21)$$

where $\tau_m = \rho_f V_m / \dot{m}$ is the characteristic residence time for either volume, and V_m is the corresponding volume. Given the subsystem transfer functions in Eqs. (17) and (21), the total system transfer function is finally given by

$$Tr_T(f) = Tr_{upper}(f) Tr_p(f) Tr_{lower}(f). \quad (22)$$

V. EXPERIMENTS AND RESULTS

Experiments were performed in order to determine experimental transfer functions as functions of the flow rate, bed diameter, bed length, sphere diameter, and number of spheres within the packed bed. As depicted in Fig. 3, sinusoidal temperature oscillations were imposed on the control stream upstream of the attenuator using a plate heat exchanger and an on-off flow controller. The on-off flow controller modulated the flow rate of a chilled water stream that passed through the primary side of the heat exchanger; this in turn produced oscillations in temperature in the control stream passing through the secondary side. Control stream input and output temperatures at the attenuator were measured with thermistors connected to a digital multimeter

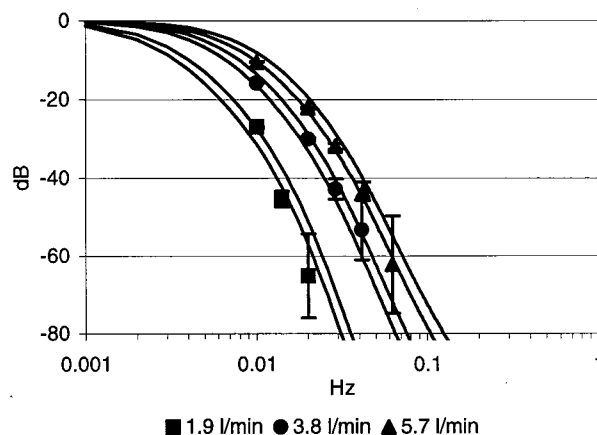


FIG. 4. Measured and theoretical attenuator transfer functions vs the frequency, including envelopes of uncertainty for theoretical curves and bars of uncertainty at measured points, for the 150 mm diam tube containing 10 000 6.4 mm spheres, subject to flow rates of 1.9, 3.8, and 5.7 l/min and a variation in rms inlet temperature of 4.1 dB.

(DMM), with thermistor resistances read from the DMM via a general purpose interface bus (GPIB) interface and converted to temperatures using the manufacturer's equations and coefficients. Input and output temperatures were then converted to frequency space via fast Fourier transforms and, in turn, were used to compute the transfer function at each input frequency.

In the first set of experiments, experimental device transfer functions for a 150 mm diam, 120 mm long packed bed containing 10 000 (N), 6.4 mm (D) diameter steel spheres were measured at three different flow rates. The results, along with theoretical device transfer functions, are given in Fig. 4. Considering qualitative features exhibited by the data, the most apparent is the decrease in spectral attenuation with an increase in flow rate. This can be explained using the packed bed and mixing volume subsystem transfer functions given by Eqs. (20) and (21). Specifically, within the packed bed subsystem, since the total thermal resistance, R , is roughly proportional to $\dot{m}^{-0.6}$ [see Eq. (9) and note that since Re_D is proportional to \dot{m} , h is proportional to $\dot{m}^{0.6}$; in addition, note and that the conductive resistance, R_{cond} , is fixed], then $\eta_L \zeta = (\dot{m} c_p R)^{-1}$ is approximately proportional to $\dot{m}^{-0.4}$. Thus, spectral attenuation within the packed bed decreases with an increase in \dot{m} . Similarly, referring to Eq. (21), it is seen that since τ_m is roughly proportional to \dot{m}^{-1} , spectral attenuation within the upper and lower volumes likewise decreases with an increase in \dot{m} . The largest disagreement between theoretical and measured results occurs for the smallest flow rate, 1.9 l/min, where the root mean square (rms) deviation is 7 dB. The rms deviations for the 3.8 and 5.7 l/min flows through the bed are both approximately 2 dB. Measurement uncertainty at low frequencies is negligibly small due to the large input and output amplitudes, whereas large measurement uncertainty occurs in the range of 60 dB, where output signals are close to the instrumentation noise floor.¹

In order to examine the capability of the model to predict effects produced by changes in the number of spheres, N , the

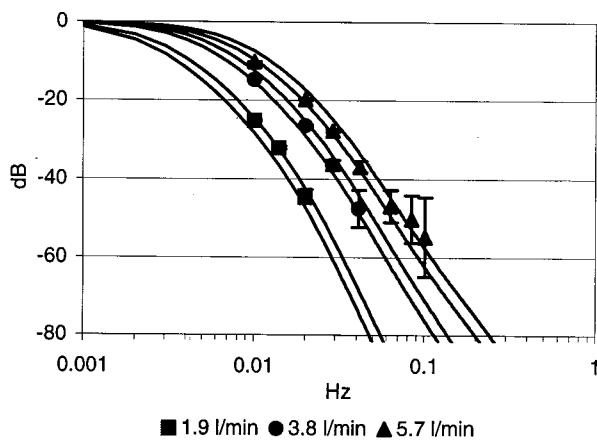


FIG. 5. Measured and theoretical attenuator transfer functions vs the frequency, including envelopes of uncertainty for theoretical curves and bars of uncertainty at measured points, for the 150 mm diam tube containing 5000 6.4 mm spheres, subject to flow rates of 1.9, 3.8, and 5.7 l/min and a variation in rms inlet temperature of 2.2 dB.

same set of experiments as those described above were repeated, with N reduced from 10 000 to 5000. The results, presented in Fig. 5, show that the model is capable of accurately predicting transfer function sensitivity to N . In this case, rms deviation between theory and experiment is approximately 2 over all three experiments.

In order to examine the effects of bed length and bed diameter on attenuation, the first set of experiments described above was repeated using a 270 mm long, 100 mm diam packed bed containing 10 000, 6.4 mm diam spheres. In order to reduce measurement uncertainties, the magnitude of input temperature oscillations was increased from approximately 0.2 K (used in the experiments reported in Figs. 4 and 5) to approximately 2 K; this had the effect of lowering the (effective) transfer function noise floor. As indicated in Fig. 6, the rms deviations between theoretical and measured attenuation are approximately 2.4, 0.4, and 1.3 dB for the 1.9, 3.8, and 5.7 l/min flow rates, respectively. The same decrease in spectral attenuation with an increase in flow rate that is observed in the first set of experiments is also seen here.

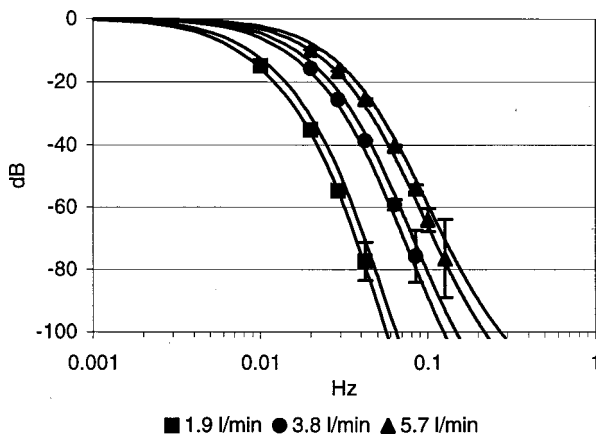


FIG. 6. Measured and theoretical attenuator transfer functions vs the frequency, including envelopes of uncertainty for theoretical curves and bars of uncertainty at measured points, for the 100 mm diam tube containing 10 000 6.4 mm spheres, subject to flow rates of 1.9, 3.8, and 5.7 l/min and a variation in rms inlet temperature of 1.5 dB.

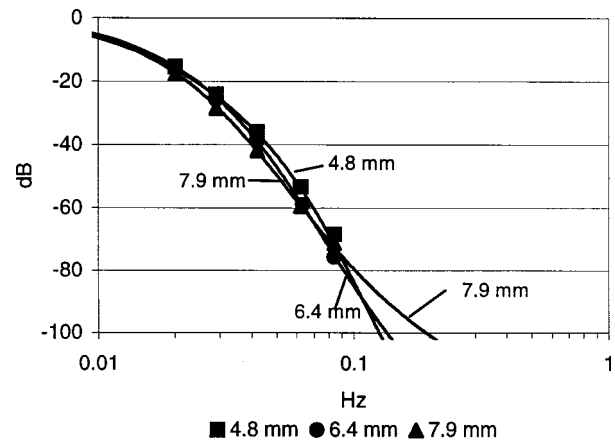


FIG. 7. Measured and theoretical attenuator transfer functions vs the frequency for the 100 mm diam tube containing 20 000 4.8, 10 000 6.4, and 5000 7.9 mm spheres, subject to a 3.8 l/min flow rate and a variation in rms inlet temperature of 1.0 dB.

Improved agreement between measurements and theory is also apparent and likely reflects the use of larger input temperature oscillations.

In the last set of experiments, the combined effects of sphere count and sphere diameter were examined, with the results shown in Fig. 7. The rms deviations between theoretical and experimental transfer functions for three combinations of sphere diameter and count, $(D, N) = (4.8 \text{ mm}, 20\,000)$, $(6.4 \text{ mm}, 10\,000)$, and $(7.9 \text{ mm}, 5000)$, are 1.6, 0.4, and 0.6 dB, respectively. The average rms deviation for these three sets of data is 0.87 dB, thus indicating that over a range of four orders of magnitude, the theoretical model matches experimental results by better than a factor of 1.1. Close examination of the plots reveals an apparent decrease in packed bed asymptotic attenuation for the three respective combinations of (D, N) : $(4.8 \text{ mm}, 20\,000)$, $(6.4 \text{ mm}, 10\,000)$, and $(7.9 \text{ mm}, 5000)$. This trend is indicated by the increased flattening in each of the curves at frequencies greater than approximately 0.08 Hz. This can be explained as follows. Since h is approximately proportional to $D^{-0.4}$ [refer to Eq. (9)], then $R_{\text{conv}} \propto N^{-1} D^{-2.4}$. In addition, since $R_{\text{cond}} \propto (ND)^{-1}$, then $R = R_{\text{cond}} + R_{\text{conv}} \propto N^{-1} (D^{-1}$

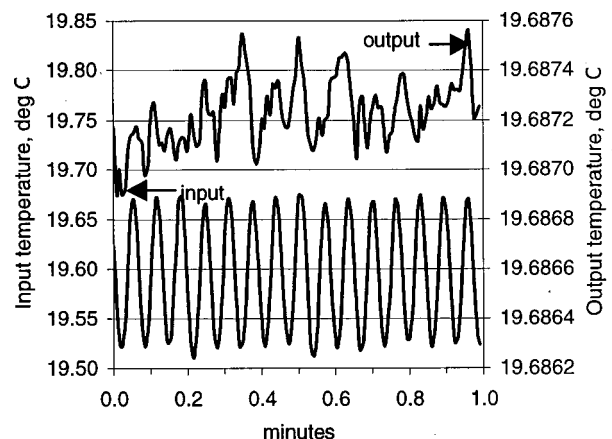


FIG. 8. Packed bed attenuator input and output temperatures for the 100 mm diam tube containing 10 000 6.4 mm spheres, subject to a 3.8 l/min flow rate and variations in input temperature of approximately 150 mK.

+ $D^{-2.4} \approx (ND)^{-1}$. Thus, since asymptotic attenuation is inversely proportional to R [see Eq. (19)], then asymptotic attenuation goes as ND , consistent with the plots and data shown. [Although not shown, it is found that asymptotic attenuation within the packed bed does indeed decrease in this manner. Note too that gradual leveling off of system attenuation strictly reflects attenuation within the packed bed; transfer function plots associated with the upper and lower volumes are never concave upward. Refer to Fig. 2.] For clarity, theoretical uncertainties are not included in Fig. 7.

Figure 8 shows the performance of the packed bed thermal attenuator in the time domain. The variations in input temperature have a period of approximately 4 s and a peak-to-peak amplitude of 150 mK, whereas the variation in output temperature is only 0.6 mK. This represents the characteristic performance of the attenuator as would be observed when the device is used to generate a high-stability chilled water supply for precise control of the temperature.

In summary, Figs. 4–7 depict theoretical transfer functions for 12 combinations of flow and attenuator parameters, along with 52 measured values of the transfer function taken in the frequency range of 0.01–0.1 Hz. The rms deviation between theory and experiment over this frequency range is approximately 2.5 dB. This degree of agreement between measured data and theoretical models is consistent with previous results¹ and thus extends application of the previously developed modeling approach to direct contact packed bed attenuators.

APPENDIX: TREATMENT OF UNCERTAINTY

The theoretical envelopes that represent model uncertainty are calculated via Eq. (22) using measured mean flow rates along with associated estimated uncertainties. Measurement uncertainty is estimated by first expressing the system transfer function as the ratio of the amplitudes of the variations in output and input temperature,

$$Tr(f) = \frac{T_{out}(f)}{T_{in}(f)}. \tag{A1}$$

The uncertainty in the transfer function is then estimated by assuming that individual uncertainties are independent and normally distributed, so that

$$\sigma_{Tr} = \left[\left(\frac{\partial Tr}{\partial T_{out}} \right)^2 \sigma_{T_{out}}^2 + \left(\frac{\partial Tr}{\partial T_{in}} \right)^2 \sigma_{T_{in}}^2 \right]^{1/2}, \tag{A2}$$

where

$$\sigma_{T_{out}}^2 = \sigma_{T_{out}}^2(f) = (S_t \sigma_T)^2 + [T_{out}(f) \sigma_s]^2 \tag{A3}$$

and

$$\sigma_{T_{in}}^2 = \sigma_{T_{in}}^2(f) = (S_t \sigma_T)^2 + [T_{in}(f) \sigma_s]^2, \tag{A4}$$

and $\sigma_T (= 0.25 \Omega)$ is the thermistor measurement uncertainty, $S_t (= 1.77 \times 10^{-3} \text{ K}/\Omega)$ is the nominal thermistor sensitivity, and $\sigma_s (= 5 \times 10^{-4} \text{ K/K})$ is the uncertainty of S_t .

¹K. Lawton, S. Patterson, and R. Keanini, *ASME J. Heat Transfer* **123**, 796 (2001).
²K. Lawton, S. Patterson, and V. Badami, *Proceedings of the 15th Annual Meeting of the ASPE*, Scottsdale, AZ, 2000, pp. 280–283.
³R. D. Cutkosky and B. F. Field, *IEEE Trans. Instrum. Meas.* **23**, 295 (1974).
⁴H. S. Lee, S. H. Yang, and N. S. Chung, *Rev. Sci. Instrum.* **61**, 1329 (1990).
⁵J. Dratler, *Rev. Sci. Instrum.* **45**, 1435 (1974).
⁶R. D. Esman and D. L. Rode, *Rev. Sci. Instrum.* **54**, 1368 (1983).
⁷R. D. Cutkosky and R. S. Davis, *Rev. Sci. Instrum.* **52**, 1403 (1981).
⁸R. B. Strem, B. K. Das, and S. C. Greer, *Rev. Sci. Instrum.* **52**, 1705 (1981).
⁹G. I. Williams and W. A. House, *J. Phys. E* **14**, 755 (1981).
¹⁰R. J. Miller and H. F. Gleeson, *Meas. Sci. Technol.* **14**, 904 (1994).
¹¹D. Sarid and D. S. Cannell, *Rev. Sci. Instrum.* **45**, 1082 (1974).
¹²M. E. Harvey, *Rev. Sci. Instrum.* **39**, 13 (1968).
¹³H. Ogasawara, *Rev. Sci. Instrum.* **57**, 3048 (1986).
¹⁴Z. Priel, *J. Phys. E* **11**, 27 (1978).
¹⁵M. C. L. Iglesias and M. Baron, *Rev. Sci. Instrum.* **61**, 2245 (1990).
¹⁶H. Ogasawara and J. Nishimura, *Appl. Opt.* **21**, 1156 (1982).
¹⁷H. Ogasawara and J. Nishimura, *Appl. Opt.* **22**, 655 (1983).
¹⁸P. H. Sydenham and G. C. Collins, *J. Phys. E* **8**, 311 (1975).
¹⁹K. Kazihara, A. Yoshihiro, T. Sonoda, and R. Ueda, *Rev. Sci. Instrum.* **68**, 1743 (1997).
²⁰G. M. Cushman, J. C. Mather, and D. J. Fixsen, *Rev. Sci. Instrum.* **68**, 4596 (1997).
²¹F. Kreith and M. Bohn, *Principles of Heat Transfer*, 5th ed. (PWS, New York, 1997), p. 443.
²²F. Incropera and D. DeWitt, *Introduction to Heat Transfer*, 4th ed. (Wiley, New York, 1990).